Burkholderia pseudomallei rapidly infects the brain stem and spinal cord via the trigeminal nerve after intranasal inoculation

St John, James A.; Walkden, Heidi; Nazareth, Lynn; Beagley, Kenneth W.; Ulett, Glen C.; Batzloff, Michael R.; Beacham, Ifor R.; Ekberg, Jenny A

Published in:
Infection and Immunity

DOI:
10.1128/IAI.00361-16

AMERICAN SOCIETY FOR MICROBIOLOGY | Infection and Immunity

Burkholderia pseudomallei Rapidly Infects the Brain Stem and Spinal Cord via the Trigeminal Nerve after Intranasal Inoculation

James A. St. John,[a,e] Heidi Walkden,[a,b] Lynn Nazareth,[a,b] Kenneth W. Beagley,[c] Glen C. Ulett,[d,e] Michael R. Batzloff,[e] Ifor R. Beacham,[e] Jenny A. K. Ekberg[a,b,c]

Eskitis Institute for Drug Discovery, Griffith University, Brisbane, Queensland, Australia[a]; Faculty of Health Sciences and Medicine, Bond University, Gold Coast, Queensland, Australia[b]; Institute for Health and Biomedical Innovation, Queensland University of Technology, Brisbane, Queensland, Australia[c]; School of Medical Science, Griffith University, Gold Coast, Queensland, Australia[d]; Institute for Glycomics, Griffith University, Gold Coast, Queensland, Australia[e]

Infection with *Burkholderia pseudomallei* causes melioidosis, a disease with a high mortality rate (20% in Australia and 40% in Southeast Asia). Neurological melioidosis is particularly prevalent in northern Australian patients and involves brain stem infection, which can progress to the spinal cord; however, the route by which the bacteria invade the central nervous system (CNS) is unknown. We have previously demonstrated that *B. pseudomallei* can infect the olfactory and trigeminal nerves within the nasal cavity following intranasal inoculation. As the trigeminal nerve projects into the brain stem, we investigated whether the bacteria could continue along this nerve to penetrate the CNS. After intranasal inoculation of mice, *B. pseudomallei* caused low-level localized infection within the nasal cavity epithelium, prior to invasion of the trigeminal nerve in small numbers. *B. pseudomallei* rapidly invaded the trigeminal nerve and crossed the astrocytic barrier to enter the brain stem within 24 h and then rapidly progressed over 2,000 μm into the spinal cord. To rule out that the bacteria used a hematogenous route, we used a capsule-deficient mutant of *B. pseudomallei* that does not survive in the blood and found that it also entered the CNS via the trigeminal nerve. This suggests that the primary route of entry is via the nerves that innervate the nasal cavity. We found that actin-mediated motility could facilitate initial infection of the olfactory epithelium. Thus, we have demonstrated that *B. pseudomallei* can rapidly infect the brain and spinal cord via the trigeminal nerve branches that innervate the nasal cavity.

Bacterial infections of the brain can be extremely severe with high rates of morbidity and mortality (1), highlighting the need for elucidating the mechanisms of central nervous system (CNS) infection. The nasal cavity is innervated by the olfactory and trigeminal nerves (cranial nerves 1 and 5, respectively), both of which constitute potential direct conduits to the brain: the olfactory nerve terminates in the olfactory bulb, whereas the trigeminal nerve makes direct contact with the brain stem.

We and others have shown that olfactory glia, olfactory ensheathing cells (OECs), play an essential role in preventing microbial invasion of the olfactory nerve by phagocytosing microorganisms (2, 3). The glia of the trigeminal nerve are Schwann cells, which are also phagocytic and remove debris after peripheral nerve injury as well as at least some types of bacteria (3, 4). Thus, glial cells in the nerves that innervate the nasal cavity constitute potentially critical defenses against microbial invasion of the brain.

To date, only a few microorganisms have been suggested as being able to invade the olfactory or trigeminal nerves. These are *Burkholderia pseudomallei* (5, 6), *Chlamydia pneumoniae* (7), *Streptococcus pneumoniae* (8), *Neisseria meningitidis* (9), *Salmonella enterica*, and *Nocardia cyriacigeorgica* (10), and the amoeboflagellate *Naegleria fowlerii* (11). We have shown that *B. pseudomallei* can invade the brain via the olfactory nerve in mice (6), and that infection led to the death of olfactory neurons and their axons, resulting in the formation of open channels lined by OECs. The open channels provided the bacteria with a direct conduit into the olfactory bulb in the forebrain. *B. pseudomallei* also penetrated branches of the trigeminal nerve locally in the nasal cavity (6), leading to the possibility that the infection could progress further along the trigeminal nerve and potentially involve the brain stem or even the spinal cord. Invasion of the trigeminal nerve is well documented as a translocation pathway by which viruses such as the herpes simplex virus invade the CNS (12–15). In addition to *B. pseudomallei*, only one bacterial species has been suggested, but not directly shown, to infect the trigeminal nerve: *Listeria monocytogenes*, the most common cause of bacterial meningitis, with a mortality rate of up to 40 to 60% (16, 17). However, direct evidence of any bacteria using this pathway to invade the brain stem is so far lacking.

Infection with *B. pseudomallei* causes melioidosis, which has an estimated worldwide prevalence of around 165,000 cases each year, with an annual death toll of 89,000 (18). *B. pseudomallei* is endemic in 45 countries and is predicted to also be endemic in another 34 countries, where it is considered to be underreported (18). In northern Australia and Southeast Asia, which are the regions where it is most prevalent, the disease has mortality rates of up to 20% and 40%, respectively (19). In humans, the neurologi-

Received 29 April 2016 **Returned for modification** 15 May 2016
Accepted 27 June 2016

Accepted manuscript posted online 5 July 2016

Citation St John JA, Walkden H, Nazareth L, Beagley KW, Ulett GC, Batzloff MR, Beacham IR, Ekberg JAK. 2016. *Burkholderia pseudomallei* rapidly infects the brain stem and spinal cord via the trigeminal nerve after intranasal inoculation. Infect Immun 84:2681–2688. doi:10.1128/IAI.00361-16.

Editor: G. H. Palmer, Washington State University

Address correspondence to Ifor R. Beacham, i.beacham@griffith.edu.au, or Jenny A. K. Ekberg, jekberg@bond.edu.au.

J.A.S.J. and H.W. contributed equally to this article.

Supplemental material for this article may be found at http://dx.doi.org/10.1128/IAI.00361-16.

cal form of melioidosis involves infection of the brain stem, which may progress to the spinal cord (20–22). As the trigeminal nerve innervates the face and nasal region and connects directly to the brain stem, we hypothesized that bacteria migrate along this nerve to penetrate the brain stem and thereby bypass the blood-brain and blood-cerebrospinal fluid barriers. The aim of the present study was therefore to determine whether *B. pseudomallei* uses the trigeminal nerve as a route of entry into the spinal cord.

MATERIALS AND METHODS

Bacterial strains and growth conditions. *B. pseudomallei* strain MSHR520 (previously strain 08) (23) is a clinical isolate from a human case of melioidosis, donated by Bart Currie (Menzies School of Health Research, Darwin, Australia). Allele replacement mutants of MSHR520 lacking capsule (MSHR520 Δ*cap*) or capsule and BimA (MSHR520 Δ*cap* Δ*bimA*) have been previously described (5, 24). The *fliC* in-frame deletion mutant, derived from MSHR520, was constructed as previously described (24); the deletion encompassed nucleotides 33937849 and 33938757 with reference to the nucleotide sequence of K96243, locus BPSL3319 (25). *B. pseudomallei* cells were grown with aeration in liquid lysogeny broth (LB) media.

Animals. Adult transgenic S100β-DsRed mice (26) were inoculated intranasally with *B. pseudomallei* strain MSHR520 ($n = 10$ animals) or MSHR520 Δ*cap* ($n = 5$ animals) by placing a 5-μl droplet of bacteria into each nostril. The inoculum contained 3×10^5 stationary-phase cells resuspended in phosphate-buffered saline (PBS). Control mice were given PBS alone; 11 noninfected and 10 infected mice were analyzed. Blood and spleen examined 24 h postinoculation with wild-type or Δ*cap* bacteria showed <5 CFU in blood (per ml) and spleen (per spleen) for the Δ*cap* strain, compared with 34 CFU and 10^3 CFU for the wild-type bacteria ($n = 5$ animals for each of Δ*cap* strain and wild-type bacteria). Procedures were approved by ESK/03/15/AEC Griffith University and the University Animal Ethics Committee at Queensland University of Technology under the guidelines of the Australian Commonwealth Office of the Gene Technology Regulator.

Tissue preparation and sectioning. Mice were sacrificed by a lethal intraperitoneal injection of sodium pentobarbitone (Lethabarb), and tissue was fixed in 4% paraformaldehyde in PBS overnight at 4°C and decalcified in 20% EDTA. For whole-mount preparations, the superior skull and brain were removed, and the trigeminal nerve was dissected out. Specimens were embedded in optimal cutting temperature (OCT) medium and frozen, and coronal and sagittal sections (30 μm) were cut on a cryostat.

Immunohistochemistry. Immunohistochemistry was performed as previously described (6). Whole-mount specimens were incubated with rabbit anti-*B. pseudomallei* polyclonal antibodies (5, 6) for 3 days at 4°C and then incubated with goat anti-rabbit Alexa Fluor 488-conjugated secondary antibodies. Cryostat sections were incubated with either anti-*B. pseudomallei* polyclonal antibodies or goat anti-glial fibrillary acidic protein (anti-GFAP) antibodies (ab53554; Abcam), followed by either donkey anti-rabbit Alexa Fluor 488-conjugated secondary antibodies or donkey anti-goat Alexa Fluor 488-conjugated secondary antibodies; some sections were incubated with 4′,6-diamidino-2-phenylindole (DAPI).

Image capture. Images were captured using an Olympus BX50 epifluorescence microscope, an Olympus SZX16 epifluorescent stereo microscope, or an Olympus FV1000 laser scanning confocal microscope. For comparison of control antibody staining using the confocal microscope, the same image capture settings, laser intensity, and focal depth were used. Captured images were color balanced uniformly across the field of view with Adobe Photoshop CC 2015 and compiled into panels with Adobe Illustrator CC 2015.

Competition assays. The Δ*cap* Δ*bimA* and Δ*cap* Δ*fliC* mutants of *B. pseudomallei* were tested for their capacity to infect upper respiratory tract tissues in BALB/c mice (nasal mucosa-associated lymphoid tissue [NALT] and olfactory mucosa [OM]) and olfactory bulb (OB) by competition assays (27) against an isogenic Δ*cap* but bioluminescent *B. pseudomallei* Tn*7 omp-lux* Δ*cap* strain (5). The Δ*cap lux*$^+$ derivative was also used in a competition assay against the isogenic nonbioluminescent Δ*cap lux*-negative strain to ascertain any possible *in vivo* fitness disadvantage of the *lux*$^+$ strain. Each of the two strains used in a competition assay was grown in LB medium and mixed in a ratio of 1:1, and 3×10^5 CFU used for inoculation of mice. The ratio of each strain in the inoculum, the input ratio (the ratio of the test strain to the Δ*cap lux*$^+$ strain), was determined by plating appropriate dilutions on LB medium containing streptomycin and counting the ratio of Lux$^-$ to Lux$^+$ colonies. Likewise, the output ratio in NALT, olfactory epithelium, and olfactory bulb was determined following dissection and homogenization of tissues and plating. The Lux phenotype was determined by imaging of the plates with a Bertholt Night-Owl camera system. The competition index (CI) was determined by dividing the output ratio by the input ratio. It may be noted that the Δ*cap lux*$^+$ strain exhibited no significant fitness disadvantage when competed *in vitro* over at least 15 generations in LB medium (containing no antibiotics) against the isogenic (nonbioluminescent) Δ*cap* strain: CIs of 0.79 and 1.10 were obtained in two independent experiments. Competition indices *in vivo* were approximately 2 (1.9 ± 0.47, 2.0 ± 0.33, and 1.45 ± 0.24 for NALT, olfactory epithelium, and olfactory bulb, respectively), indicating a slight disadvantage of the Lux$^+$ strain *in vivo*. Five independent experiments were performed. Each *lux* mutant "test" bacterial genotype (Δ*cap*, Δ*cap* Δ*fliC*, and Δ*cap* Δ*bimA*) and each tissue was examined in duplicate, triplicate, or quadruplet experiments: the Δ*cap* Δ*bimA* strain, for example, was used in 4 experiments for the OM, 3 for the NALT, and 2 for the OB. The total number of animals examined (n [between 6 and 24]) for each tissue represents the cumulative number of animals for all the relevant experiments (for example $n = 8$, 24, and 9 for NALT, OM, and OB, respectively, in the case of the Δ*cap* Δ*bimA* strain). Blood was taken by heart puncture from each animal, in addition to the relevant organs, and plated to determine CFU. In all cases, colonies were not detected at 24 h postinfection (<5 CFU/ml). Statistical analysis was performed using Prism software with a one-way analysis of variance (ANOVA) followed by *post hoc* Bonferroni's test, with the alpha value set at 0.05.

Data availability. All data and methods are contained within this article.

RESULTS

***Burkholderia pseudomallei* penetrates the nasal epithelium to invade the trigeminal nerve.** This study was undertaken to investigate whether *B. pseudomallei* could invade the brain stem via the trigeminal nerve branches that innervate the nasal cavity (Fig. 1A). Transgenic reporter S100β-DsRed mice (26) were used, in which all glial cells, including Schwann cells, express the red fluorescent protein DsRed. Using these mice, the trigeminal nerve, in which individual axons are surrounded by Schwann cells, can be easily detected (for example, see Fig. 1E). Adult S100β-DsRed mice were intranasally inoculated with wild-type *B. pseudomallei* and then analyzed after 24 h.

Within the caudal nasal cavity, the dorsal region is lined with olfactory epithelium, which is primarily found along the septum and around the turbinates (nasal concha), an elongated spiral bone shelf inside the nasal cavity (Fig. 1B). In adult healthy noninfected control mice, the olfactory epithelium remained intact and smooth in appearance, with no exudate present within the nasal cavity (data not shown). In mice that had been inoculated with *B. pseudomallei*, the olfactory epithelium reacted to the presence of the bacteria by mild crenellation and the production of exudate within the nasal cavity (Fig. 1B). Immunohistochemistry using antibodies against *B. pseudomallei* revealed the presence of bacteria within the nasal cavity and olfactory epithelium (Fig. 1C).

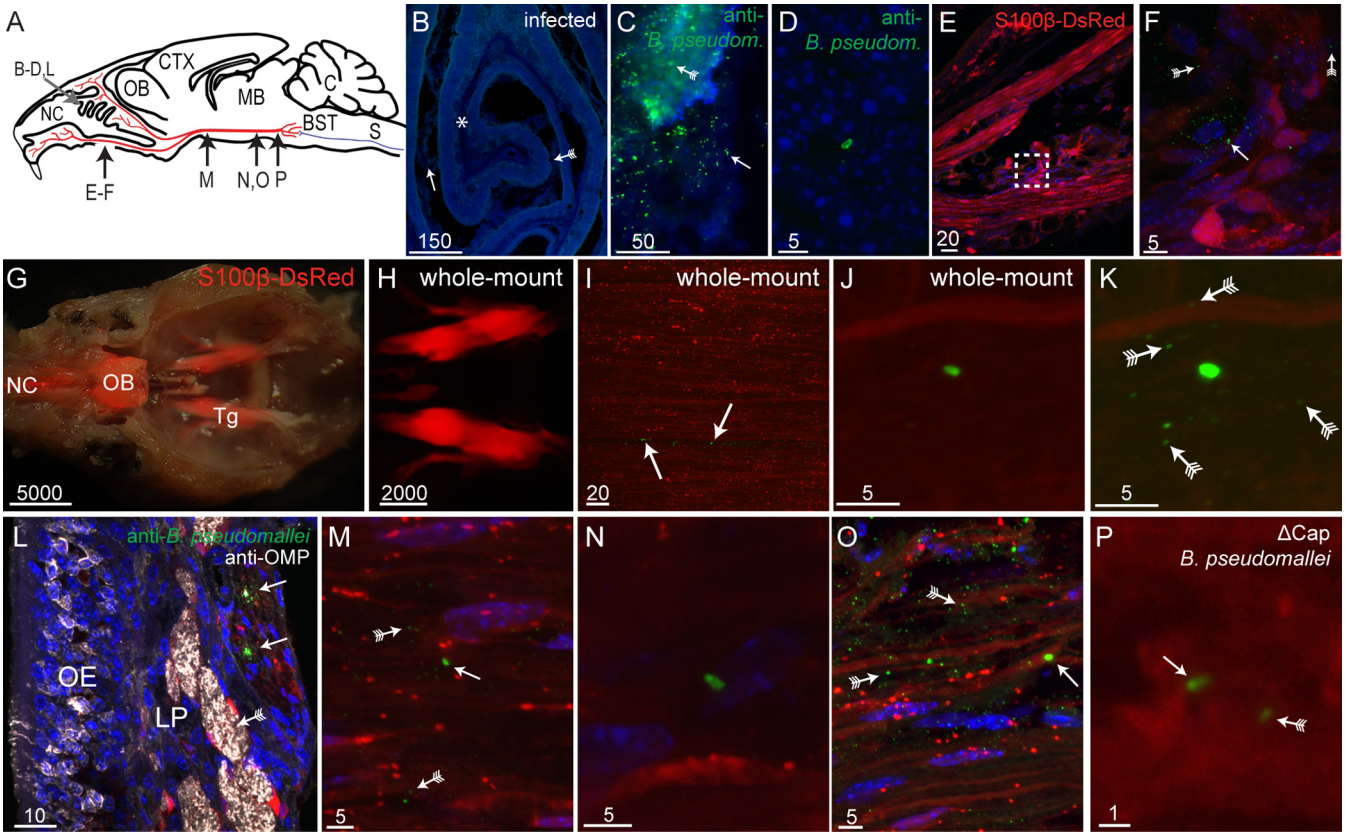

FIG 1 *Burkholderia pseudomallei* infects the trigeminal nerve via the nasal cavity. (A) Schematic drawing of a sagittal mouse brain section showing the locations of various panels: nasal cavity (NC), olfactory bulb (OB), cerebral cortex (CTX), midbrain (MB), cerebellum (C), brain stem (BST [blue]), spinal cord (S [blue]), and trigeminal nerve (red). (B and C) Tissue sections from mice infected with *B. pseudomallei*; nuclei are stained with DAPI. (B) Coronal view of a turbinate with widespread crenellation of the epithelium (fletched arrow) and exudate (arrow) within the nasal cavity. An asterisk shows the location of the image shown in panel D. (C) *B. pseudomallei* immunolabeling (green) within degraded olfactory epithelium (fletched arrow) and NC (arrow). (D) *B. pseudomallei* immunolabeling (green) within the lamina propria underlying the epithelium. (E) Sagittal view of the nasal region showing branches of the trigeminal nerve (red, S100β-DsRed; blue, DAPI); the boxed region is shown in panel F. (F) *B. pseudomallei* (arrow) near the trigeminal nerve, and associated particles immunoreactive for anti-*B. pseudomallei* antibodies (fletched arrows). (G to K) Whole-mount preparations of mouse heads. (G) Dorsal view of a whole-mount preparation of a mouse head, with the brain removed. The image is a merge of a bright-field image and a fluorescent image showing DsRed expression in the nasal cavity (NC), olfactory bulb (OB), and trigeminal nerves (Tg). (H) Fluorescent whole-mount image showing the structure of the trigeminal nerves while still present within the mouse head. (I) Trigeminal nerve after removal from the whole-mount mouse head and immunolabeled with anti-*B. pseudomallei* antibodies showing *B. pseudomallei* (arrows) within the nerve. (J) High-magnification view showing a *B. pseudomallei* rod within the whole-mount trigeminal nerve. (K) Same image shown in panel J with green fluorescence overexposed, revealing the presence of the associated particles. (Fletched arrows show some of the particles.) (L to P) Bacteria present throughout the trigeminal nerve in cryostat sections. (L) The olfactory mucosa consists of the olfactory epithelium (OE) and lamina propria (LP), olfactory nerve fascicles immunolabeled with anti-OMP antibodies (white [fletched arrow]), and a trigeminal nerve branch with Schwann cells that express DsRed with *B. pseudomallei* immunolabeling (arrows). (M) *B. pseudomallei* (arrow) within the trigeminal nerve midway (rostral-caudal) along the nerve. Associated particles can also be seen (fletched arrows). (N) *B. pseudomallei* present within the trigeminal nerve toward the caudal end of the nerve. (O) *B. pseudomallei* (arrow) and associated particles (fletched arrows) were localized to discrete patches within the trigeminal nerve. (P) *B. pseudomallei* Δ*cap* rod (arrow) with a fluorescent particle (arrow with tail) within the caudal region of the trigeminal nerve. Scale bars are in micrometers.

Individual bacteria were occasionally present within the lamina propria, the connective tissue layer found below the olfactory epithelium (Fig. 1D). Branches of the trigeminal nerve are present within the lamina propria, and *B. pseudomallei* cells were found proximal to trigeminal nerve branches (Fig. 1E and F). In addition to *B. pseudomallei* rods, multiple immunoreactive punctate particles that measured less than 1 μm in diameter were detected around the rods (Fig. 1F). These have been previously associated with the presence of *B. pseudomallei* in inoculated mice (6) and may be outer membrane vesicles (28) or products of the degradation of *B. pseudomallei*.

***Burkholderia pseudomallei* infection spreads to the caudal region of the trigeminal nerve.** The branches of the trigeminal nerve converge at the trigeminal ganglions, where they connect with the brain stem (Fig. 1A). To elucidate whether bacteria migrate along the trigeminal nerve, whole-mount imaging was used. In whole-mount heads of S100β-DsRed mice, the trajectory of the trigeminal nerve to the caudal region of the cranial cavity could be visualized due to the S100β-DsRed-expressing Schwann cells (Fig. 1G and H). Whole-mount immunohistochemistry revealed *B. pseudomallei* cells within patches and in small numbers along the trigeminal nerve; some of the patches of *B. pseudomallei* appeared to be present within a single Schwann cell (Fig. 1I). Higher magnification of the whole-mount nerve revealed *B. pseudomallei* rods, which were often found in isolation (Fig. 1J). The associated focal areas of punctate particles of green fluorescent staining that

were observed in Fig. 1F were also present; however, they were only visible if the fluorescence was overexposed, due to the depth of tissue (Fig. 1K). (In panel K, some particles are indicated by fletched arrows.)

We next examined tissue sections using higher-magnification confocal microscopy. Immunolabeling of cryostat sections of the olfactory mucosa was performed to confirm that *B. pseudomallei* invaded the trigeminal nerve. Within the olfactory mucosa that lines the nasal cavity, immunolabeled *B. pseudomallei* cells were detected within a branch of the trigeminal nerve within the lamina propria (Fig. 1L). To confirm the identity of the olfactory versus the trigeminal nerve fascicles, immunohistochemistry using antibodies against olfactory marker protein (OMP) was performed as OMP is selectively expressed by olfactory sensory neurons and their axons but not axons of the trigeminal nerve. The immunolabeling showed that the OMP-positive olfactory nerve fascicles were more apical than the trigeminal nerve fascicles. In this strain of mice, *B. pseudomallei* immunolabeling was only detected within the trigeminal nerve branches and not in the olfactory nerve branches. Also of note was that the olfactory epithelium remained relatively intact, as evidenced by the presence of numerous olfactory sensory neurons (Fig. 1L).

By using sagittal sections of the entire heads of mice, the trigeminal nerves were examined along their trajectory from the nasal cavity to the merge into the brain stem. Immunolabeling revealed that isolated individual *B. pseudomallei* rods were present throughout the nerve (Fig. 1M and N). The immunoreactive fluorescent particles were also present, although they were more noticeable toward the rostral end of the trigeminal nerve (Fig. 1M). *B. pseudomallei* cells were present in patches along the trigeminal nerve and separated by regions of the nerve where no bacteria or immunoreactive particles were detected (data not shown). These observations were consistent with those from the whole-mount analysis (Fig. 1G to K). Nuclear staining revealed that the numbers of host cells in the areas of bacteria invasion did not increase (Fig. 1O), suggesting that circulating immune cells had not been recruited to the infected area.

To investigate whether *B. pseudomallei* cells were localized only to the trigeminal nerve, areas adjacent to the trigeminal nerve and the entire brain were also analyzed. These analyses showed the presence of *B. pseudomallei* and associated immunoreactive particles was exclusive to the trigeminal nerve; the bacteria were not detected in other areas (data not shown). To verify that immunolabeling was specific for *B. pseudomallei*, sections of uninfected mice were also immunolabeled for *B. pseudomallei*, and the nasal region, trigeminal nerve, and adjacent brain tissue were analyzed. Importantly, no immunoreactivity was observed in any of the noninfected mice (data not shown).

To verify that *B. pseudomallei* cells were not penetrating the brain via alternative routes (in particular, via the blood-brain-barrier), an acapsular mutant strain (Δ*cap*) of *B. pseudomallei* was used. The capsule is required for survival and persistence in the blood (6, 29). We found that the *B. pseudomallei* Δ*cap* mutant similarly penetrated the trigeminal nerve and reached the caudal region of the nerve 24 h following inoculation (Fig. 1P). Since this strain cannot survive in the blood, it is highly unlikely to have entered the brain via hematogenous spread.

***Burkholderia pseudomallei* infection progresses into the brain stem.** We next examined the brain stem for the presence of the bacteria to determine if infection spreads to the CNS following intranasal inoculation. The trigeminal nerve projects to the brain stem, which then connects with the spinal cord (Fig. 2A and B). The protective barrier around the CNS, the glia limitans, comprises astrocytes that express GFAP (Fig. 2C) and clearly delineates the border between the peripheral and central nervous systems. *B. pseudomallei* was detected within the most caudal region of the trigeminal nerve (peripheral nervous system [Fig. 2D]) and within the brain stem (CNS [Fig. 2E]).

***Burkholderia pseudomallei* infection penetrates the spinal cord.** The brain stem connects directly with the spinal cord (Fig. 2A), with the division between the brain stem and spinal cord being easily identified by the smaller diameter of the nervous tissue at the rostral spinal cord (Fig. 2F). The transition from brain stem to spinal cord can also be identified by a change in the appearance of the nervous tissue, reflected in different cell types and layers (Fig. 2G). Since the spinal cord connects directly with the end of the brain stem, analysis of the spinal cord for the presence of *B. pseudomallei* was performed to investigate whether bacteria could migrate from the brain stem to the spinal cord. Within the spinal cord closest to the brain stem, multiple immunoreactive particles were present in small patches (Fig. 2H). Other areas within the same tissue section contained no immunoreactive bacteria or particles (data not shown). This correlates with our observations of the trigeminal nerve and suggests that *B. pseudomallei* infection progresses along the spinal cord either in very small patches or as isolated individual bacteria. The spinal cords of control noninfected mice were also immunolabeled with anti-*B. pseudomallei* antibodies, and immunoreactivity was not detected (data not shown). The immunoreactivity was observed in several mice ($n = 4$); however, it is of interest to note that immunoreactive areas were never detected toward the edges of the spinal cord, where GFAP-positive astrocytes were present; bacterial staining was only detected within the deeper layers of the spinal cord. Further down the spinal cord, *B. pseudomallei* rods were detected without the typically associated immunoreactive particles (Fig. 2I and J, see Movie S1 in the supplemental material). Overall, it appeared that fewer *B. pseudomallei* cells were present within the spinal cord than in the trigeminal nerve. For mice that exhibited immunoreactivity for *B. pseudomallei* within the spinal cord, we examined the nasal cavity for signs of infection. Some mice that had bacteria in the spinal cord had widespread infection within the nasal cavity, while other mice had very little signs of infection, with minor disruption to the caudal epithelium (Fig. 2K). The total rate of infection progression from the nasal cavity to the deepest region in the spinal cord where bacteria were detected was 0.9 mm per h, corresponding to 22 mm in 24 h.

Role of bacterial motility. The movement of bacteria within the olfactory and trigeminal nerve fascicles (5, 6; this report) raises the question of whether it is passive or involves bacterial motility. We therefore considered the possible role of actin-mediated motility, which requires the *B. pseudomallei* protein BimA (30), or of polar flagella, which requires the flagellin structural gene (FliC) (31).

Accordingly, competition indices (CIs) were determined in mixed infections of BALB/c mice between *bimA* or *fliC* mutants and the wild type as a measure of the role of BimA or FliC, respectively, in infection of the upper respiratory tract. All strains were additionally capsule deficient (Δ*cap*) to preclude infection via blood. The *lux* operon was used to mark one strain, and competition between this strain and the *lux*-negative parent strain (MSHR520 Δ*cap*) was included as a control. The results indicate

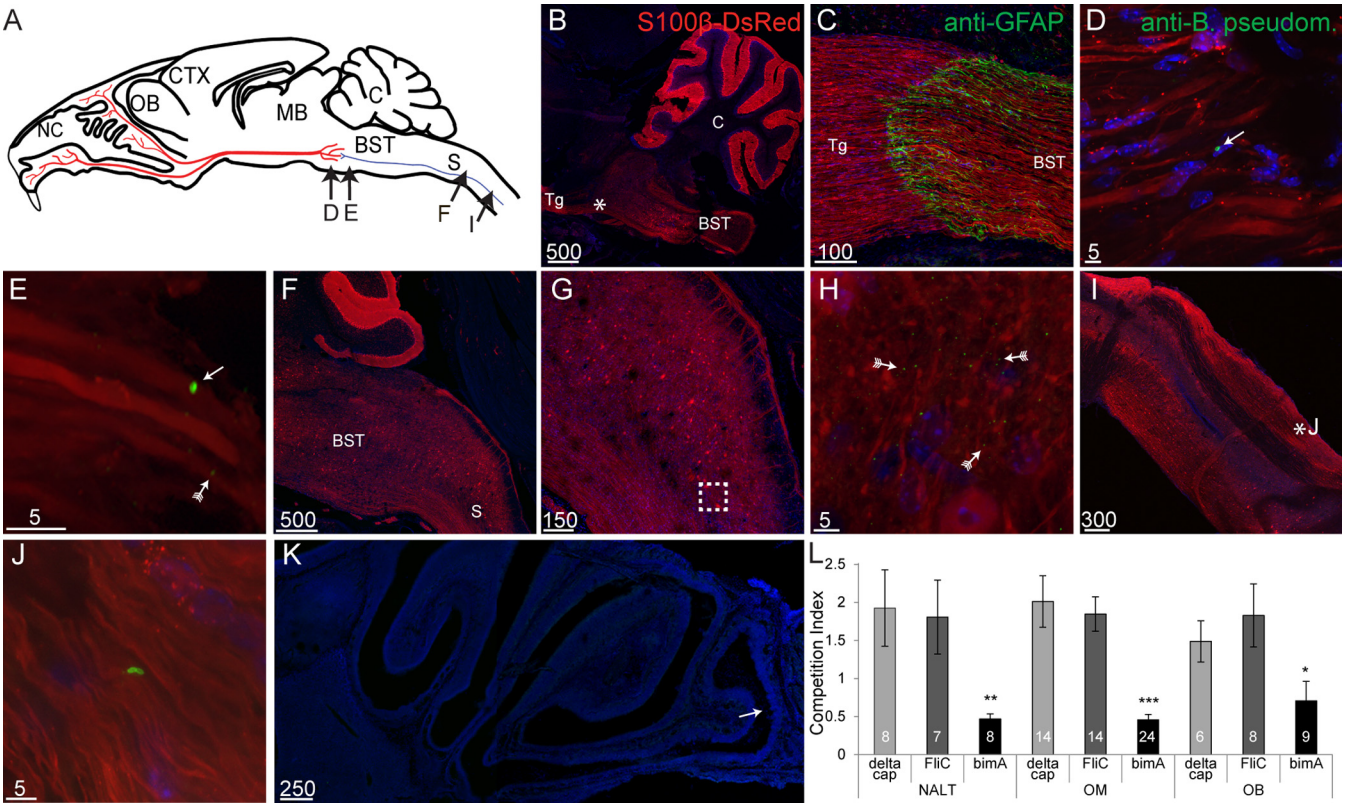

FIG 2 *B. pseudomallei* infection progresses from the trigeminal nerve into the spinal cord. (A) Sagittal schematic drawing of a mouse brain showing the location of various panels. (B) Composition of multiple sagittal images showing the cerebellum (C), brain stem (BST), and the end of the trigeminal nerve (Tg). The asterisked area is shown in panel D. (C) Low-power image showing the merge between the trigeminal nerve (Tg) and the brain stem (BST) separated by the astrocytic glia limitans (anti-GFAP [green]). (D) High-power sagittal image showing a *B. pseudomallei* rod (arrow) present in trigeminal nerve just rostral of the merge between the trigeminal nerve and the brain stem. (E) High-power image showing a *B. pseudomallei* rod (arrow) with a fluorescent particle (arrow with tail) caudal to the merge between the trigeminal nerve and brain stem. (F) Low-power image showing the transition from brain stem (BST) to spinal cord (S). (G) Low-power image illustrating the structural changes seen throughout the spinal cord. The area within the dashed square is magnified in panel H. (H) High-power image of the spinal cord showing multiple immunoreactive particles (green [fletched arrow]) associated with *B. pseudomallei* bacteria. (I) Low-power view of the spinal cord; the asterisked area is shown in panel J. (J) High-power sagittal image of two *B. pseudomallei* rods within the spinal cord (see Movie S1 in the supplemental material). (K) Nasal cavity of a mouse in which *B. pseudomallei* were detected in the spinal cord. There was little evidence of infection within the nasal cavity, with only a small region in the caudal recess showing signs of infection. Scale bars are in micrometers. (L) Competition indices of actin and flagellum mutant strains. Mice were inoculated with MSHR520 Δ*cap*, MSHR520 Δ*cap* Δ*fliC*, and MSHR520 Δ*cap* ΔBimA mutant strains, each together with the MSHR520 Δ*cap lux*$^+$ strain. Tissues from the nasal-associated lymphoid tissue (NALT), olfactory mucosa (OM), and olfactory bulb (OB) were analyzed to determine the competition index. Error bars show standard errors of the means, and *n* values are shown within the columns. *, $P < 0.05$, **, $P < 0.01$, and ***, $P < 0.001$, significantly different in comparison to the MSHR520 Δ*cap* and MSHR520Δ*cap* Δ*fliC* strains, by one-way ANOVA with *post hoc* Bonferroni's test.

that while FliC is not involved, CIs for infection of nasal mucosa-associated lymphoid tissue, olfactory mucosa, and the olfactory bulb are significantly reduced in the *bimA* strain (Fig. 2L). Thus, BimA plays a role in infection of upper respiratory tract tissue, presumably via actin-mediated cell-to-cell dissemination, and in infection of the outer layer of the olfactory bulb within the cranial cavity.

Summary of results. In summary, the results of this study show that intranasal inoculation with *B. pseudomallei* leads to infection of the trigeminal nerve without evidence of extensive infection of the nasal epithelium. Once within the confines of the trigeminal nerve, bacteria crossed the glia limitans, penetrated the CNS, and then continued into the spinal cord (Fig. 3).

DISCUSSION

We have demonstrated that *B. pseudomallei*, which causes melioidosis, can enter the CNS (brain and spinal cord) via the nasal branches of the trigeminal nerve. Our findings are consistent with clinical studies of melioidosis. Neurological melioidosis frequently involves the brain stem (21, 22, 32), and while less frequently reported, neurological melioidosis can affect the spinal cord, causing paraplegia (20). In one pediatric case, it was suggested that partial paralysis of the foot may have resulted from bacterial invasion of the spinal cord via a nerve root pathway secondary to a skin lesion. In a second pediatric case, skin lesions on the face were suggested to have resulted in trigeminal nerve invasion (33). Hence our results, in providing evidence of direct invasion of the brain stem and spinal cord secondary to trigeminal nerve invasion, are consistent with human clinical manifestations of neurological melioidosis.

In our previous study, we demonstrated local, peripheral, infection of the distal trigeminal nerve branches in the nasal epithelium (6). The bacteria were restricted to empty conduits encased by Schwann cells, as the trigeminal axons had been destroyed by the infection. In this study, once bacteria had penetrated the tri-

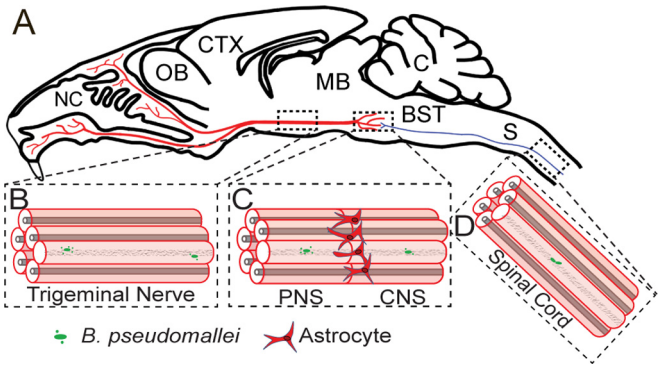

FIG 3 Schematic representation of the mechanism by which *B. pseudomallei* invades the CNS. (A) Schematic drawing of a sagittal mouse head showing the overall structure of the brain, trigeminal nerve (red), brain stem (BST), and spinal cord (S). (B) Magnified region within the trigeminal nerve. Axon degradation (gray) is restricted to a small portion of the nerve. *B. pseudomallei* cells were isolated in small numbers, often individually, with more immunoreactive particles observed toward the rostral end of the trigeminal nerve. (C) The transition between the trigeminal nerve (peripheral nervous system) and the brain stem (CNS) is defined by a layer of astrocytes, forming the glia limitans barrier. *B. pseudomallei* cells crossed this barrier and were detected within the brain stem. (D) *B. pseudomallei* rods were found deep within the spinal cord.

geminal nerve, they were present in small numbers and in discrete patches. The low level of infection, together with limited immunological surveillance in the CNS, may preclude a major immunological response. This is consistent with two well-described features of infection by *B. pseudomallei*. First, significant numbers of the population in the two main regions of endemicity (tropical Australia and Thailand) are seropositive, although the seropositivity rates in these two regions differ greatly (34). However, although indicating infection by *B. pseudomallei*, there is great uncertainty regarding the relationship between such prior infection and current latent infection (34). Second, latency following disease with subsequent recrudescence (sometimes decades later) is described in a minority of cases (34, 35). Such patterns of subclinical infection are consistent with low-level invasion of the brain stem and spinal cord. It is of interest that bacteria can cause restricted destruction of a small number of axons, as patients who develop clinical neurological symptoms do not always have detectable foci of infection or indications of pyogenic infection, even after autopsy (22). This suggests that low-level infection can produce the clinical neurological symptoms, possibly through the destruction of key axonal pathways. An alternative route by which bacteria can reach the brain is via hematogenous spread and crossing the blood-brain barrier and/or cerebrospinal fluid barrier. We show here that the Δ*cap* strain can still penetrate the trigeminal nerve, suggesting that the trigeminal nerve is indeed the primary route by which the bacteria infect the CNS.

The method by which bacteria move along the empty trigeminal, or olfactory, nerve fascicles is uncertain, but could involve bacterial motility. The apparent role of BimA in infection of the olfactory bulb may be related either (i) to movement along the olfactory nerve through open channels or (ii) to the means of access to the nerves. Considering that BimA is unlikely to be directly involved in movement within the nerve fascicles themselves, then passive movement is rendered more likely. With regard to the latter, infection of the nasal mucosa-associated lymphoid tissue and olfactory mucosa is significantly reduced in the *bimA* strain; reduced olfactory mucosal infection would presumably cause reduced infection of the olfactory nerve fascicles, and hence of the olfactory bulb, since the bacteria invade the olfactory bulb via the olfactory nerve fascicles (6). Similarly, spread via the trigeminal nerve fascicles could be influenced by BimA-facilitated infection of the olfactory mucosa in order to gain access to the trigeminal nerve endings; alternatively BimA-mediated uptake by Schwann cells and cell-to-cell spread may facilitate entry to the nerve fascicle. Significantly, our data showing that absence of BimA results in reduced olfactory bulb infection are in accord with clinical data strongly suggesting a link between BimA function and neurological melioidosis (36). There are two alleles of *bimA* extant in *B. pseudomallei*: one, $bimA_{Bp}$, typical of the majority of *B. pseudomallei* isolates, and another, $bimA_{Bm}$, resembling that from *Burkholderia mallei* and present in 12.1% of Australian isolates (37). Specifically these authors (36) reported a significant association of the $bimA_{Bm}$ allele with cases of neurological melioidosis. MSHR520 contains the $bimA_{Bp}$ allele (37, 38), and it will be of interest to compare isogenic strains carrying each allele for their capacity to infect, or maintain infection of, the olfactory and trigeminal nerve fascicles. Considering that FliC and BimA are unlikely to be directly involved in movement within the nerve fascicles themselves, then passive movement is rendered more likely.

In the present study, where we used Quackenbush mice, the background of our S100β-DsRed transgenic line, the penetration of bacteria into the trigeminal nerve did not require widespread or severe infection of the nasal epithelium. Indeed, in those mice in which bacteria were detected within the brain stem and spinal cord, there was little evidence of widespread infection within the nasal cavity. It has previously been shown that there are significant differences between melioidosis infection in BALB/c mice and another inbred mouse strain, C57BL/6, with BALB/c infection mimicking acute human melioidosis and C57BL/6 infection resembling chronic infection in humans (39). Thus, it appears that the infection observed in the outbred Quackenbush mouse strain may resemble the infection in C57BL/6 mice more than the dramatic acute infection in BALB/c mice.

In summary, our results demonstrate that after intranasal inoculation, *B. pseudomallei* can, possibly aided by actin-mediated motility, infect branches of the trigeminal nerve that innervate the nasal cavity, migrate along the trigeminal nerve, and traverse the glia limitans to penetrate the brain stem and spinal cord within 24 h. Importantly, the bacterial invasion was at low levels and did not require extensive infection of the nasal epithelium, consistent with subclinical and clinical manifestations of human infection and melioidosis. These results raise the possibility that other bacteria that can cause brain and spinal cord infections could also use the trigeminal nerve as a route of direct and rapid entry into the CNS.

ACKNOWLEDGMENTS

Johana Tello Velasquez provided assistance with the immunolabeling and microscopy.

This work was supported by a grant from the National Health and Medical Research Council (no. 1020394) to I.R.B., M.B., and G.C.U., an Australian Research Council Discovery grant (no. DP150104495) to J.A.K.E., K.W.B., and J.A.S.J., and a Perry Cross Spinal Research Foundation grant to J.A.S.J. The funders had no role in study design, data collection and interpretation, or the decision to submit the work for publication.

FUNDING INFORMATION

This work, including the efforts of James A. St. John, was funded by Perry Cross Spinal Research Foundation. This work, including the efforts of Ifor R. Beacham, Michael Batzloff, and Glen C. Ulett, was funded by Department of Health | National Health and Medical Research Council (NHMRC) (APP1020394). This work, including the efforts of Jenny A. K. Ekberg, Kenneth Beagley, and James A. St. John, was funded by Australian Research Council (ARC) (DP150104495).

The funders had no role in study design, data collection and interpretation, or the decision to submit the work for publication.

REFERENCES

1. **Huppatz C, Kelly PM, Levi C, Dalton C, Williams D, Durrheim DN.** 2009. Encephalitis in Australia, 1979–2006: trends and aetiologies. Commun Dis Intell Q Rep **33:**192–197.
2. **Nazareth L, Lineburg KE, Chuah MI, Tello Velasquez J, Chehrehasa F, St John JA, Ekberg JA.** 2015. Olfactory ensheathing cells are the main phagocytic cells that remove axon debris during early development of the olfactory system. J Comp Neurol **523:**479–494. http://dx.doi.org/10.1002/cne.23694.
3. **Panni P, Ferguson IA, Beacham I, Mackay-Sim A, Ekberg JA, St John JA.** 2013. Phagocytosis of bacteria by olfactory ensheathing cells and Schwann cells. Neurosci Lett **539:**65–70. http://dx.doi.org/10.1016/j.neulet.2013.01.052.
4. **Tello Velasquez J, Watts ME, Todorovic M, Nazareth L, Pastrana E, Diaz-Nido J, Lim F, Ekberg JA, Quinn RJ, St John JA.** 2014. Low-dose curcumin stimulates proliferation, migration and phagocytic activity of olfactory ensheathing cells. PLoS One **9:**e111787. http://dx.doi.org/10.1371/journal.pone.0111787.
5. **Owen SJ, Batzloff M, Chehrehasa F, Meedeniya A, Casart Y, Logue CA, Hirst RG, Peak IR, Mackay-Sim A, Beacham IR.** 2009. Nasal-associated lymphoid tissue and olfactory epithelium as portals of entry for *Burkholderia pseudomallei* in murine melioidosis. J Infect Dis **199:**1761–1770. http://dx.doi.org/10.1086/599210.
6. **St John JA, Ekberg JA, Dando SJ, Meedeniya AC, Horton RE, Batzloff M, Owen SJ, Holt S, Peak IR, Ulett GC, Mackay-Sim A, Beacham IR.** 2014. *Burkholderia pseudomallei* penetrates the brain via destruction of the olfactory and trigeminal nerves: implications for the pathogenesis of neurological melioidosis. mBio **5:**e00025-14. http://dx.doi.org/10.1128/mBio.00025-14.
7. **Little CS, Joyce TA, Hammond CJ, Matta H, Cahn D, Appelt DM, Balin BJ.** 2014. Detection of bacterial antigens and Alzheimer's disease-like pathology in the central nervous system of BALB/c mice following intranasal infection with a laboratory isolate of *Chlamydia pneumoniae*. Front Aging Neurosci **6:**304. http://dx.doi.org/10.3389/fnagi.2014.00304.
8. **van Ginkel FW, McGhee JR, Watt JM, Campos-Torres A, Parish LA, Briles DE.** 2003. Pneumococcal carriage results in ganglioside-mediated olfactory tissue infection. Proc Natl Acad Sci U S A **100:**14363–14367. http://dx.doi.org/10.1073/pnas.2235844100.
9. **Sjolinder H, Jonsson AB.** 2010. Olfactory nerve—a novel invasion route of *Neisseria meningitidis* to reach the meninges. PLoS One **5:**e14034. http://dx.doi.org/10.1371/journal.pone.0014034.
10. **Dando SJ, Mackay-Sim A, Norton R, Currie BJ, St John JA, Ekberg JA, Batzloff M, Ulett GC, Beacham IR.** 2014. Pathogens penetrating the central nervous system: infection pathways and the cellular and molecular mechanisms of invasion. Clin Microbiol Rev **27:**691–726. http://dx.doi.org/10.1128/CMR.00118-13.
11. **Cervantes-Sandoval I, Serrano-Luna JdJ, Meza-Cervantez P, Arroyo R, Tsutsumi V, Shibayama M.** 2009. *Naegleria fowleri* induces MUC5AC and pro-inflammatory cytokines in human epithelial cells via ROS production and EGFR activation. Microbiology **155:**3739–3747. http://dx.doi.org/10.1099/mic.0.030635-0.
12. **Beers DR, Henkel JS, Schaefer DC, Rose JW, Stroop WG.** 1993. Neuropathology of herpes simplex virus encephalitis in a rat seizure model. J Neuropathol Exp Neurol **52:**241–252. http://dx.doi.org/10.1097/00005072-199305000-00008.
13. **Enquist LW.** 2012. Five questions about viral trafficking in neurons. PLoS Pathog **8:**e1002472. http://dx.doi.org/10.1371/journal.ppat.1002472.
14. **Kristensson K.** 2011. Microbes' roadmap to neurons. Nat Rev Neurosci **12:**345–357. http://dx.doi.org/10.1038/nrn3029.
15. **Salinas S, Schiavo G, Kremer EJ.** 2010. A hitchhiker's guide to the nervous system: the complex journey of viruses and toxins. Nat Rev Microbiol **8:**645–655. http://dx.doi.org/10.1038/nrmicro2395.
16. **Jin Y, Dons L, Kristensson K, Rottenberg ME.** 2001. Neural route of cerebral *Listeria monocytogenes* murine infection: role of immune response mechanisms in controlling bacterial neuroinvasion. Infect Immun **69:**1093–1100. http://dx.doi.org/10.1128/IAI.69.2.1093-1100.2001.
17. **Vazquez-Boland JA, Kuhn M, Berche P, Chakraborty T, Dominguez-Bernal G, Goebel W, Gonzalez-Zorn B, Wehland J, Kreft J.** 2001. *Listeria* pathogenesis and molecular virulence determinants. Clin Microbiol Rev **14:**584–640. http://dx.doi.org/10.1128/CMR.14.3.584-640.2001.
18. **Limmathurotsakul D, Golding N, Dance DA, Messina JP, Pigott DM, Moyes CL, Rolim DB, Bertherat E, Day NP, Peacock SJ, Hay SI.** 2016. Predicted global distribution of and burden of melioidosis. Nat Microbiol **1:**15008. http://dx.doi.org/10.1038/nmicrobiol.2015.8.
19. **White NJ.** 2003. Melioidosis. Lancet **361:**1715–1722. http://dx.doi.org/10.1016/S0140-6736(03)13374-0.
20. **Bartley PP, Pender MP, Woods ML, II, Walker D, Douglas JA, Allworth AM, Eisen DP, Currie BJ.** 1999. Spinal cord disease due to melioidosis. Trans R Soc Trop Med Hyg **93:**175–176. http://dx.doi.org/10.1016/S0035-9203(99)90299-7.
21. **Currie BJ, Fisher DA, Howard DM, Burrow JN.** 2000. Neurological melioidosis. Acta Trop **74:**145–151. http://dx.doi.org/10.1016/S0001-706X(99)00064-9.
22. **Woods ML, II, Currie BJ, Howard DM, Tierney A, Watson A, Anstey NM, Philpott J, Asche V, Withnall K.** 1992. Neurological melioidosis: seven cases from the Northern Territory of Australia. Clin Infect Dis **15:**163–169. http://dx.doi.org/10.1093/clinids/15.1.163.
23. **Brown NF, Beacham IR.** 2000. Cloning and analysis of genomic differences unique to *Burkholderia pseudomallei* by comparison with *B. thailandensis*. J Med Microbiol **49:**993–1001. http://dx.doi.org/10.1099/0022-1317-49-11-993.
24. **Horton RE, Grant GD, Matthews B, Batzloff M, Owen SJ, Kyan S, Flegg CP, Clark AM, Ulett GC, Morrison N, Peak IR, Beacham IR.** 2013. Quorum sensing negatively regulates multinucleate cell formation during intracellular growth of *Burkholderia pseudomallei* in macrophage-like cells. PLoS One **8:**e63394. http://dx.doi.org/10.1371/journal.pone.0063394.
25. **Holden MT, Titball RW, Peacock SJ, Cerdeno-Tarraga AM, Atkins T, Crossman LC, Pitt T, Churcher C, Mungall K, Bentley SD, Sebaihia M, Thomson NR, Bason N, Beacham IR, Brooks K, Brown KA, Brown NF, Challis GL, Cherevach I, Chillingworth T, Cronin A, Crossett B, Davis P, DeShazer D, Feltwell T, Fraser A, Hance Z, Hauser H, Holroyd S, Jagels K, Keith KE, Maddison M, Moule S, Price C, Quail MA, Rabbinowitsch E, Rutherford K, Sanders M, Simmonds M, Songsivilai S, Stevens K, Tumapa S, Vesaratchavest M, Whitehead S, Yeats C, Barrell BG, Oyston PC, Parkhill J.** 2004. Genomic plasticity of the causative agent of melioidosis, *Burkholderia pseudomallei*. Proc Natl Acad Sci U S A **101:**14240–14245. http://dx.doi.org/10.1073/pnas.0403302101.
26. **Windus LC, Claxton C, Allen CL, Key B, St John JA.** 2007. Motile membrane protrusions regulate cell-cell adhesion and migration of olfactory ensheathing glia. Glia **55:**1708–1719. http://dx.doi.org/10.1002/glia.20586.
27. **Osorio CG, Crawford JA, Michalski J, Martinez-Wilson H, Kaper JB, Camilli A.** 2005. Second-generation recombination-based in vivo expression technology for large-scale screening for *Vibrio cholerae* genes induced during infection of the mouse small intestine. Infect Immun **73:**972–980. http://dx.doi.org/10.1128/IAI.73.2.972-980.2005.
28. **Kulp A, Kuehn MJ.** 2010. Biological functions and biogenesis of secreted bacterial outer membrane vesicles. Annu Rev Microbiol **64:**163–184. http://dx.doi.org/10.1146/annurev.micro.091208.073413.
29. **Reckseidler-Zenteno SL, DeVinney R, Woods DE.** 2005. The capsular polysaccharide of *Burkholderia pseudomallei* contributes to survival in serum by reducing complement factor C3b deposition. Infect Immun **73:**1106–1115. http://dx.doi.org/10.1128/IAI.73.2.1106-1115.2005.
30. **Stevens MP, Stevens JM, Jeng RL, Taylor LA, Wood MW, Hawes P, Monaghan P, Welch MD, Galyov EE.** 2005. Identification of a bacterial factor required for actin-based motility of *Burkholderia pseudomallei*. Mol Microbiol **56:**40–53. http://dx.doi.org/10.1111/j.1365-2958.2004.04528.x.
31. **DeShazer D, Brett PJ, Carlyon R, Woods DE.** 1997. Mutagenesis of *Burkholderia pseudomallei* with Tn5-OT182: isolation of motility mutants and molecular characterization of the flagellin structural gene. J Bacteriol **179:**2116–2125.
32. **Koszyca B, Currie BJ, Blumbergs PC.** 2004. The neuropathology of melioidosis: two cases and a review of the literature. Clin Neuropathol **23:**195–203.

33. **McLeod C, Morris PS, Bauert PA, Kilburn CJ, Ward LM, Baird RW, Currie BJ.** 2015. Clinical presentation and medical management of melioidosis in children: a 24-year prospective study in the Northern Territory of Australia and review of the literature. Clin Infect Dis **60:**21–26. http://dx.doi.org/10.1093/cid/ciu733.
34. **Currie BJ.** 2015. Melioidosis: evolving concepts in epidemiology, pathogenesis, and treatment. Semin Respir Crit Care Med **36:**111–125. http://dx.doi.org/10.1055/s-0034-1398389.
35. **Ngauy V, Lemeshev Y, Sadkowski L, Crawford G.** 2005. Cutaneous melioidosis in a man who was taken as a prisoner of war by the Japanese during World War II. J Clin Microbiol **43:**970–972. http://dx.doi.org/10.1128/JCM.43.2.970-972.2005.
36. **Sarovich DS, Price EP, Webb JR, Ward LM, Voutsinos MY, Tuanyok A, Mayo M, Kaestli M, Currie BJ.** 2014. Variable virulence factors in *Burkholderia pseudomallei* (melioidosis) associated with human disease. PLoS One **9:**e91682. http://dx.doi.org/10.1371/journal.pone.0091682.
37. **Sitthidet C, Stevens JM, Chantratita N, Currie BJ, Peacock SJ, Korbsrisate S, Stevens MP.** 2008. Prevalence and sequence diversity of a factor required for actin-based motility in natural populations of *Burkholderia* species. J Clin Microbiol **46:**2418–2422. http://dx.doi.org/10.1128/JCM.00368-08.
38. **Johnson SL, Bishop-Lilly KA, Ladner JT, Daligault HE, Davenport KW, Jaissle J, Frey KG, Koroleva GI, Bruce DC, Coyne SR, Broomall SM, Li PE, Teshima H, Gibbons HS, Palacios GF, Rosenzweig CN, Redden CL, Xu Y, Minogue TD, Chain PS.** 2015. Complete genome sequences for 59 *Burkholderia* isolates, both pathogenic and near neighbor. Genome Announc **3:**e00159-15. http://dx.doi.org/10.1128/genomeA.00159-15.
39. **Leakey AK, Ulett GC, Hirst RG.** 1998. BALB/c and C57Bl/6 mice infected with virulent *Burkholderia pseudomallei* provide contrasting animal models for the acute and chronic forms of human melioidosis. Microb Pathog **24:**269–275. http://dx.doi.org/10.1006/mpat.1997.0179.